THE EFFECTS OF ATMOSPHERIC DUST ON THE SEASONAL VARIATION OF MARTIAN SURFACE TEMPERTURE

R. J. Wilson , *Geophysical Fluid Dynamics Laboratory, Princeton, NJ (John.Wilson@noaa.gov),* and **M. D. Smith,** *NASA Goddard Space Flight Center, Greenbelt, MD., USA.*

Introduction: The daily and seasonal variation of surface temperature is a central element in the description of martian climate. Surface thermal inertia and albedo are critical boundary inputs for simulating surface temperature in Mars general circulation models (MGCMs). Thermal inertia (TI) is also of intrinsic interest as it may be related to regolith properties such as particle size and surface character and so high spatial resolution is desirable. The recent mapping of TI at very high (0.25°) spatial resolution was achieved by fitting a thermal model to surface temperature observations [*Putzig et al*. 2005]. However, varying atmospheric opacity (dust and water ice clouds) can significantly influence the estimated TI field and this effect was not fully compensated for. Opacity has a direct effect on surface temperatures, acting to increase morning temperature and decrease afternoon temperature. Additionally, opacity within the 7.8 and 23 μm spectral regions contributes to the sensed radiation that is used to infer surface temperature, thus increasing the apparent thermal inertia. We are particularly interested in assessing the influence of dust aerosol and water ice clouds on simulated surface temperature and using differences between simulated and observed temperatures to constrain our representation of atmospheric opacity. We have used MGS TES surface temperature, albedo and thermal inertia estimates [*Christensen et al*. 2001; *Putzig et al*. 2005] to derive improved thermal inertia fields suitable for use in versions of the GFDL MGCM with resolutions from 5x6° to 2x2.4°. In deriving TI at these coarser resolutions, we are able to bin TES data with sufficient temporal resolution to relate the evolution of observed morning and afternoon temperatures to variations in atmospheric opacity. By construction, the newly fitted TI field allows the MGCM to reproduce the observed morning and afternoon temperatures in seasons and locations where our assumptions of atmospheric opacity are well founded. Differences between observed and simulated temperatures largely reflect the influence of dust and/or water ice clouds not accounted for in a given simulation. In a companion presentation [*Wilson et al*., this workshop], we describe the mapping of nighttime water ice clouds by identifying their radiative influence on nighttime surface temperatures.

In this presentation we illustrate the utility of accurate modeling of surface temperatures by exploring the behavior of surface temperatures over the course of the 2001 global dust storm. The influence of dust on surface temperature is likely to play a significant role in the life cycles of local and regional scale dust storms. Sufficient surface cooling can lead to the suppression of boundary layer turbulence which may be a critical ingredient for dust lifting. Alternatively, surface cooling may promote the development of density currents on sloping topography. *Kahn* [1995] attempted to evaluate afternoon surface temperature differences within and outside of an intense local dust storm using Viking IRTM data. The MGS observations of a number of regional dust storms and the global event of 2001 provide a more extensive basis for assessing the influence of dust on both nighttime and daytime temperatures. It can be readily anticipated that the effect of dust will be strongly controlled by the aerosol optical properties. *Haberle and Jakosky* [1991] discussed the dependence of the greenhouse effect of dust on the dust particle size distribution, which influences the ratio of visible-to-infrared opacity. We consider a series of simulations with different dust columns and/or properties to obtain constraints on the dust column evolution and its optical properties during the 2001 storm.

General Circulation Model: The GFDL MGCM simulates the circulation of the Martian atmosphere with a comprehensive set of physical parameterizations [*Wilson and Hamilton*, 1996; *Wilson and Hinson*, 2004]. These include parameterizations for radiative transfer associated with CO_2 gas and aerosols. The dust aerosol fields may be either specified or allowed to evolve with the circulation following prescribed or interactive lifting at the surface. We use a 2-stream method to account for aerosol scattering and absorption when calculating radiative fluxes in the shortwave and the longwave. The relevant optical properties are the extinction cross section efficiency, Q_{ext}, the single scattering albedo, ω, and the asymmetry parameter, g. These are all functions of wavelength, and aerosol composition and size. We employ the dust radiative properties in the IR that are described by *Wolff and Clancy* [2003]. We include a calculation of the simulated T_7 and T_{23} brightness temperatures, which are the appropriate quantities to compare with the observations. The MGCM has a 12-layer soil model with a depth-dependent soil diffusivity that can be tuned to fit

the observed temperatures. In practice, we assume a uniform diffusivity for all nonpolar grid boxes. We obtain improved agreement with observed temperatures poleward of 55° by including a depth-dependent soil diffusivity to represent the thermal influence of shallow subsurface water ice, which affects the effective thermal inertia on timescales of tens of sols. This is motivated by the detection of subsurface water ice by the Mars Odyssey Gamma Ray Spectrometer (GRS). It is evident that this effect is important for realistic simulation of polar region temperatures and ice cap recession.

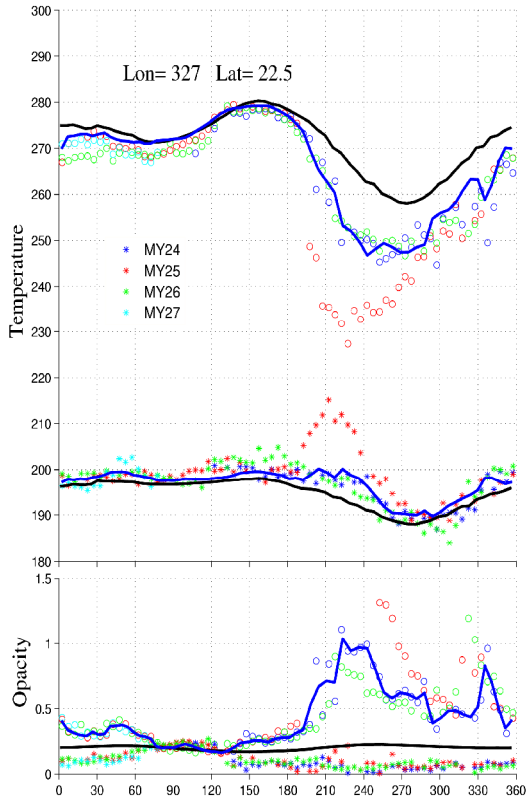

Figure 1.The seasonal variation of 2am (stars) and 2pm (circles) TES surface temperatures for a location in Chryse over 4 Mars years: MY24 (blue), MY25 (red), MY26 (green) and MY27 (cyan). The solid curves show simulated T_7 and T_{23} brightness temperatures which correspond to TES daytime and nighttime temperatures, respectively. The effect of the major dust storms at L_s= 187 and 225° is evident. (b) The seasonal variation of visible dust opacity used in the 2 simulations. Dust opacities derived from TES spectra are shown with open circles, while stars indicate retrieved ice opacity. TES IR opacities have been converted to visible opacity by a scaling factor of 2.

Best fit thermal inertia: A best fit thermal inertia field was derived through an iterative process, starting with an initial thermal inertia field [*Putzig et al.* 2005] and using a fixed albedo field [*Christensen et al.* 2001]. We used the available estimates of dust opacity when matching observed and simulated temperatures during the dust-variable perihelion season. In principle, the observed day and night temperatures are sufficient to fit both thermal inertia and albedo. We used an invariant albedo, although the evidence is clear that surface albedo does vary due to the deposition or removal of a thin layer of dust as was the case following the 2001 global dust storm. Of course, the observed albedo is a measure of the combined reflectivity of the surface and atmosphere, rather than being a property of the surface alone. Currently our TI determination is a compromise fit in some locations where a temporally variable albedo might provide a better fit to the observed temperatures. The Hellas region presents particular problems as the frequent presence of dust and water ice clouds render specifying the atmospheric state somewhat problematic. In these cases, we have weighted our fittings to seasons where we have the greatest confidence in the specification of atmospheric opacity. Figure 1 shows our ability to simulate the surface temperatures at a location in the Chyrse basin. The black and curve shows temperature from the reference simulation with fixed weak dust opacity (τ=0.15). The blue curve shows the model response to dust opacity varying according to TES dust retrievals from MY24-25. The use of observed dust opacity provides a good match over an annual cycle. It is worth noting that the dip in observed 2pm temperatures around L_s=90 may be attributed to the presence of water ice clouds, which are not accounted for in the simulation.

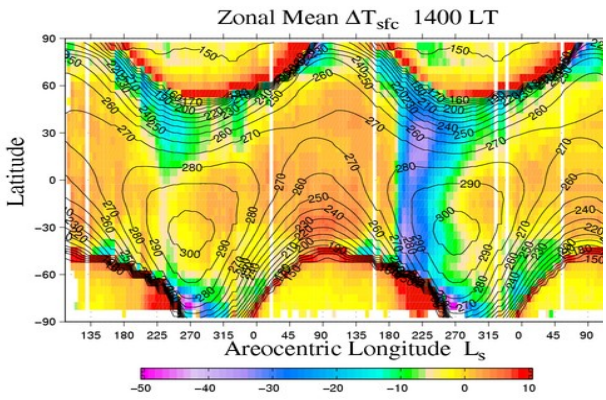

Figure 2. The seasonal evolution of zonally-averaged afternoon surface temperature from a reference MGCM simulation employing a low (τ=0.15) atmospheric dust column is shown with 10 K contour intervals. The shading indicates the temperature anomaly resulting when the reference field is subtracted from the observed TES temperatures. The cooling effect of the regional and major dust storms is clearly evident.

Zonal mean surface temperatures: Figure 2 shows the seasonal evolution of zonally-averaged 2pm surface temperature from a reference simulation representing relatively clear sky conditions (fixed dust with τ=0.15). There is a large seasonal variation in temperature that reflects the seasonal migration of the subsolar latitude and the annual variation in insolation due to the eccentric orbit. The advance and retreat of the polar CO_2 ice caps approximately follows the 155 K isotherm. Figure 2 also shows the zonally-averaged differences between TES and simulated surface temperatures. This anomaly field emphasizes the seasonal changes of observed temperatures that may be largely attributed to variations in atmospheric opacity. Temperature differences are minimal during the relatively clear NH spring/summer season when the low opacity assumed in the simulation most closely approximates that of the actual atmosphere. The effects of regional scale dust storms at L_s=225 and 320° in the first mapping year (MY24) and the 2001 dust storm at L_s=187° in the second year (MY25) are evident. The temperature differences in the immediate vicinity of the polar caps point up deficiencies in the model simulation of the CO_2 cap evolution. For example, the model does not predict a residual CO_2 cap in the SH. For the most part, temperature differences over the polar caps are due to the influence of dust and ice clouds on retrieved brightness temperatures. This effect is also significant for dust storm events and can be accounted for by comparing observed surface temperatures with either simulated T_7 and T_{23}, whichever is appropriate.

Dust Radiative Effects: The 2001 global dust storm provides a valuable opportunity to investigate the radiative influence of dust. Both the column dust opacity and the dust optical properties (SW and IR) influence the relative decrease in daytime temperatures and increase in nighttime temperatures. These effects are more or less amplified by the surface thermal inertia and albedo. For example, nighttime surface temperatures are most strongly increased in regions of low surfaced thermal inertia. Figure 3 shows the evolution of observed and simulated temperatures in the Hesperia region, using the prescribed (visible) dust column opacities indicated in the bottom panel. The red and green curves show the variation of temperatures for specified dust opacity intended to yield a good fit to the 2001 dust storm period. Two different values of visible dust asymmetry factor (g) are used to illustrate the influence of dust optical properties. Simulations 2001A and 2001D employ g= 0.45 and 0.65, respectively. Increased forward scattering allows more direct solar radiation at the surface and can ran result in unrealistically enhanced greenhouse response. The near-surface atmospheric temperatures in 2001D are distinctly warmer (10 K in the diurnal average) than those in 2001A. The observational constraints on g are not well determined, with values typically ranging from 0.55 to 0.8. Of course, these results will depend on the visible to IR opacity assumed. In our case, we considered a distribution of particles with an effective radius of 2μm, yielding a visible-to-IR ratio of 1.38. As noted by *Haberle and Jakosky* (1991), a larger ratio, appropriate for smaller dust particles, would yield a reduced greenhouse effect.

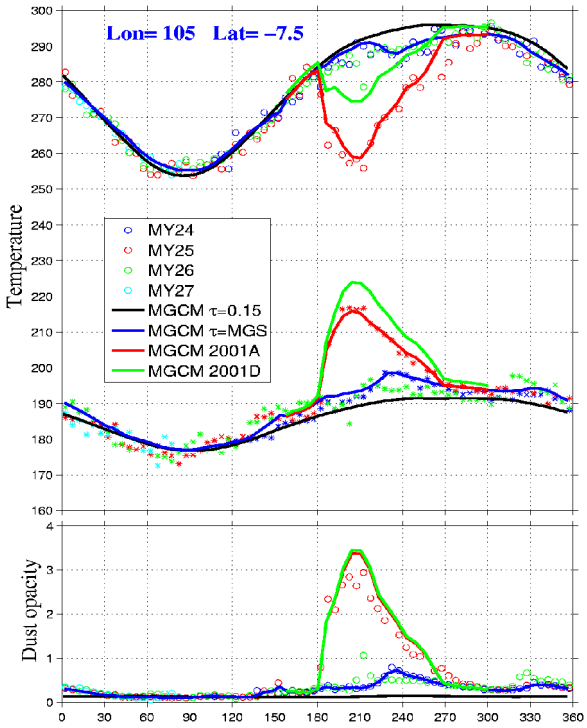

Figure 3.The seasonal variation of 2am (stars) and 2pm (circles) TES surface temperatures for a location in Hesperia over 3 Mars years: MY24 (blue), MY25 (red), and MY26 (green). The solid curves represent the corresponding temperatures from four MGCM simulations. The simulations shown in red and green differ only in the choice of dust asymmetry parameter, (g): 2001A and 2001D use values of 0.45 and 0.65, respectively. (b) The seasonal variation of visible opacity used in the 4 simulations. Open circles indicate opacity estimates derived from TES. These have been converted to visible opacity by a scaling factor of 2.

A limitation in deriving dust opacity from TES spectra is the need for a temperature contrast between the surface and the level of dominant aerosol emission [*Smith* 2004]. In practice, opacity determinations have been restricted to daytime observations where the surface temperature exceeds 215 K. During particularly dusty conditions, daytime surface temperatures are strongly suppressed while atmospheric temperatures are increased by solar absorption. At these times, the

required temperature contrast is lost and opacity is ill-determined. We can obtain an independent estimate of opacity by comparing the surface (and atmospheric) temperatures from simulations with a range of dust opacity and optical properties with the TES observations. Figure 4 shows the opacity field derived by fitting simulated afternoon temperatures to the observations. For a given choice of dust model, we carried out simulations with dust columns that bracketed the expected local column opacity. The correspondence between retrieved and fitted opacity is quite good. This technique provides opacity estimates in certain key regions such as Syria and Hellas where retrievals are missing or are questionable. It is possible to estimate opacities over the polar cap as well.

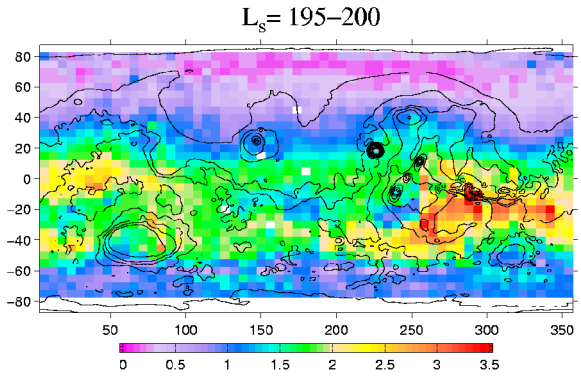

Figure 4. Spatial distribution of normalized dust column visible opacity as the 2001 dust storm is well underway. Opacities have been normalized by surface pressure to minimize the influence of topography. The opacity is derived by interpolating from a set of simulated afternoon temperatures (T_7) to fit observations.

We now consider how the choice of dust column and properties influences the simulation of atmospheric temperatures. Figure 5 shows a comparison of meridional temperature structure from two simulations with that from TES retrievals. The two simulations share the same specified dust distribution and differ only in the choice of dust visible single scattering albedo, ω, which has little influence on surface temperature. There is considerably more atmospheric absorption in Fig. 5b, providing a better match to the observed temperatures. The daytime temperature inversion within the Hellas basin is stronger and more realistic in this case. It is likely that this inversion played a significant role in the apparent cessation of active dust lifting in Hellas after the 2001 storm event was well underway [*Strausberg et al*. 2005]. While this work is not proposed as a retrieval technique for dust optical properties, it does stress the need for an appropriate choice in model simulations, to maintain consistent aspects of the thermal structure and circulation.

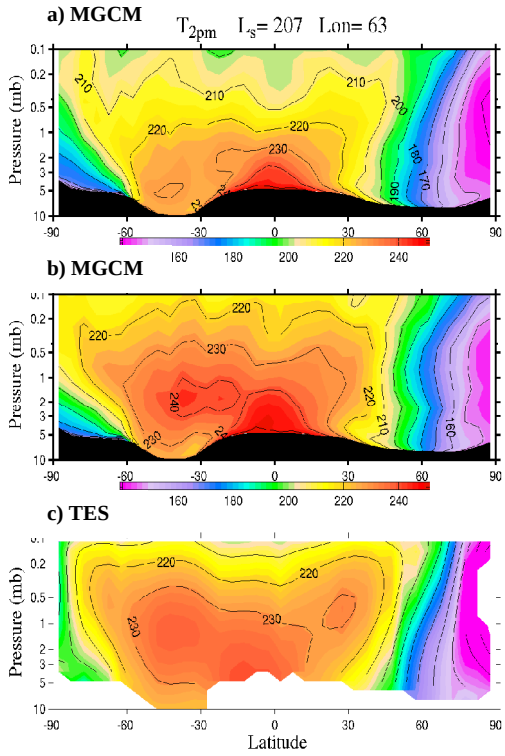

Figure 5. Meridional cross sections of 2pm temperature through the Hellas basin near the peak of the 2001 global dust storm. (a) MGCM simulation (2001A) with ω=0.92 and g= 0.45 (b) MGCM simulation (2001E) with g= 0.45 (c) TES retrievals.

References:

Christensen et al., MGS Thermal Emission Spectrometer experiment: Investigation description and surface science results, *J. Geophys. Res., 106* (E10), 23,823 - 23,872, 2001.

Haberle, R., and B.M. Jakosky, Atmospheric effects on the remote determination of thermal inertia on Mars, *Icarus, 90,* 187-204, 1991.

Hinson, D., and R.J. Wilson, Temperature inversions, thermal tides, and water ice clouds in the Martian tropics, *J. Geophys. Res., 109, E01002,* doi:10.1029/JE002129, 2004.

Kahn, R., Temperature measurements of a martian local dust storm, *J. Geophys. Res., 100,* 5265-5275, 1995.

Putzig, N.E., M.T. Mellon, K.A. Kretke, and R.E. Arvidson, Global thermal inertia and surface properties of Mars from the MGS mapping mission, *Icarus,* 173, 325-341, 2005.

Smith, M.D., Interannual variability in TES atmospheric observations of Mars during 1999-2003, *Icarus, 108,* 148-165, 2004.

Strausberg, M.J., *et al*. (2005), Observations of the initiation and evolution of the 2001 Mars global dust storm, *J. Geophys. Res., 110,* E02006, doi:10.1029/2004JE002361.

Wilson, R.J., and K.P. Hamilton, Comprehensive model simulation of thermal tides in the Martian atmosphere, *J. Atmos. Sci., 53,* 1290-1326, 1996

Wolff, M.J., and R.T. Clancy, Constraints on the size of Martian aerosols from Thermal Emission Spectrometer observations, *J. Geophys. Res., 108,* E(9), 5097, 2003.